



## Microstructure and mechanical properties of high strength Al–Zn–Mg–Cu alloys used for oil drill pipes

Chun FENG<sup>1,2</sup>, Wen-bin SHOU<sup>3</sup>, Hui-qun LIU<sup>3</sup>, Dan-qing YI<sup>3</sup>, Yao-rong FENG<sup>1,2</sup>

1. Tubular Goods Research Institute of CNPC, Xi'an 710065, China;
2. CNPC Key Laboratory for Petroleum Tubular Goods Engineering, Xi'an 710065, China;
3. School of Materials Science and Engineering, Central South University, Changsha 410083, China

Received 22 December 2014; accepted 13 April 2015

**Abstract:** Three Al–Zn–Mg–Cu alloys used for oil drill pipes (Alloy A: Al–6.9Zn–2.3Mg–1.7Cu–0.3Mn–0.17Cr; Alloy B: Al–8.0Zn–2.3Mg–2.6Cu–0.2Zr, Alloy C: Al–8.0Zn–2.3Mg–1.8Cu–0.18Zr) were studied by hardness tests, tensile tests and transmission electron microscopy (TEM). The results show that the ultimate tensile strength, yield strength and elongation for Alloys A, B and C are 736 MPa, 695.5 MPa and 7%; 711 MPa, 674 MPa and 12.5%; 740.5 MPa, 707.5 MPa and 13%, respectively after solid solution treatment ((450 °C, 2 h)+(470 °C, 1 h)) followed by aging at 120 °C for 12 h. The dominant strengthening phases in Alloy A are GPII zone and  $\eta'$  phase, the main precipitate in Alloy B is  $\eta'$  phase, and the main precipitates in Alloy C are GPI zone, GPII zone and  $\eta'$  phase, which are the reason for better comprehensive properties of Alloy C. The increase of zinc content leads to the improvement of the strength. The increase of copper content improves the elongation but slightly decreases the strength. Large second-phase particles formed by the increase in the manganese content induce a decrease in the elongation of alloys.

**Key words:** Al–Zn–Mg–Cu alloy; aging time; precipitate; microstructure; mechanical properties

### 1 Introduction

Drill pipes are a kind of the main tools in the drilling and oil industry [1]. Compared with conventional steel drill pipes, aluminum drill pipes have low density, high strength and good stress corrosion resistance; further, aluminum is non-magnetic. Therefore, aluminum alloys are now becoming ideal light structure materials for drilling [2].

The Al–Zn–Mg–Cu alloys have a strong aging strengthening effect through quenching and aging and have yield strength of up to 500 MPa at room temperature with higher impact toughness than other aluminum alloys [3]. High Zn and Mg contents reduce the ductility of the alloy and increase the brittleness. Low Cu content tends to decrease the embrittlement of the alloy and improve the plasticity, meanwhile, Cu atom can form *S* (Al<sub>2</sub>CuMg) phase with Al atoms and Mg atoms to strengthen the alloy [4]. The addition of minor Cr, Mn, Zr and Ni elements in the alloy forms some intermetallics with Al atom, and the intermetallics are

beneficial to improving the mechanical properties of the alloy. HE et al [5] and ZOU et al [6] reported that minor addition of Sc and Zr in Al–Zn–Mg–Cu alloys leads to forming Al<sub>3</sub>(Sc,Zr) particle which can greatly refine grains, inhibit recrystallization and improve the mechanical properties of the alloy.

High strength of Al–Zn–Mg–Cu alloys depends on their precipitation sequences. The usual sequences are as follows [7–10]:

Sequence 1: Supersaturated solid solution (SSS) → GP zone →  $\eta'$  phase (MgZn<sub>2</sub>) →  $\eta$  phase (MgZn<sub>2</sub>);

Sequence 2: Supersaturated solid solution (SSS) → GP zone → *T'* phase (Al<sub>2</sub>Zn<sub>3</sub>Mg<sub>3</sub>) → *T* phase (Al<sub>2</sub>Zn<sub>3</sub>Mg<sub>3</sub>).

These sequences are related to the aging temperature and Zn/Mg ratio [7,11,12]. GANG and CERESO [12] found that when the Mg content is higher than the Zn content, the main precipitate in the alloy is the *T* phase. YANG et al [7] reported that an Al–7.60Zn–2.55Mg alloy with a characteristically high Mg/Zn mole ratio can be strengthened by the *T*-phase precipitates. Currently, however, the Zn content is higher

than the Mg content in most Al–Zn–Mg–Cu alloys, the precipitation sequence is primarily the first sequence given above, and the GP zone,  $\eta'$  phase and  $\eta$  phase are still the main phases in Al–Zn–Mg–Cu alloys. ZANG et al [13] reported that a new Al–Zn–Mg–Cu alloy (Al–(7.5–8.7)Zn–(1.8–2.7)Mg–(1.4–2.1)Cu) aged at 120 °C for 24 h has superior mechanical properties compared with conventional ones, and the main phases in new alloy are GPI zone, GPII zone and  $\eta'$  phase. LI et al [14] studied the one-step aging behavior of Al–7.5Zn–1.7Mg–1.4Cu–0.12Zr alloy and found that small  $\eta'$  phase and GP zone distributed and dispersed in the matrix under the peak-aging condition. WANG et al [15] studied the one-step aging behavior of 7055 alloy and found that the GP zone and  $\eta'$  phase formed during aging significantly influenced the mechanical properties of the alloy. Recently, by the use of high-resolution transmission electron microscopy, some researchers [16,17] reported that GP– $\eta_p$  zones or  $\eta$ -precursor existed in some Al–Zn–Mg–(Cu) alloys, these two intermediate phases play an indispensable role in phase transformation.

In order to optimize the mechanical properties of aluminum drill pipes, it is necessary to investigate the effect of microstructure evolution and alloying element on mechanical properties during aging. The object of the present work is to reveal the strengthening mechanism and relationship between the microstructure and mechanical properties of the alloys by investigating the effects of aging treatment.

## 2 Experimental

The compositions of the three alloys studied are listed in Table 1. The ingots were prepared using an induction furnace. The as-cast alloys were subjected to two-step homogenization treatment ((395 °C, 12 h) + (460 °C, 32 h)). After homogenization treatment, rods of the alloys were extruded using a 300 t extrusion machine. The as-extruded samples were solid solution-treated ((450 °C, 2 h) + (470 °C, 1 h)), and then water-quenched to room temperature. After quenching, the samples were immediately aged at 120 °C for 4, 12, 24, 36 and 48 h, respectively. The Vickers hardness testing was performed on an HV–10B hardness tester with a load of 2 kg and each hardness value was obtained by averaging five measurements. The tensile tests were performed at room temperature using a DDL100 testing machine and three measurements were made to obtain the average value. The alloys were also observed using a Tecnai G2 F20 transmission electron microscope (TEM). Slices for TEM samples were cut from the aged tensile samples, and subsequently ground to less than 100  $\mu\text{m}$  and punched into 3 mm discs. The thin foils were obtained by

electrothinning at 20 V. The electrolyte was a mixture of 75% methanol and 25% nitric acid, and thinning was performed at –25 °C.

**Table 1** Compositions of studied alloys

Alloy	Mass fraction/%									
	Cu	Mg	Zn	Mn	Fe	Ni	Cr	Ti	Zr	Al
A	1.7	2.3	6.9	0.3	0.3	0.1	0.17	0	0	Bal.
B	2.6	2.3	8.0	0.05	0	0	0.04	0	0.2	Bal.
C	1.8	2.3	8.0	0.05	0	0	0.04	0.02	0.18	Bal.

## 3 Results

### 3.1 Mechanical properties

The Vickers hardness and tensile properties of Alloys A, B and C during aging at 120 °C for different time are shown in Fig. 1, Table 2 and Fig. 2. Alloys A, B and C are clearly strengthened by aging. At the early stage of aging, the hardness of the three alloys increases rapidly and approaches the first peak value after aging for 4 h. Subsequently, the hardness of Alloy C maintains at a high level for a long time. For Alloys A and B, the hardness reaches the second peak value after aging for 24 h and 36 h, respectively. The strengths of the three alloys exhibit the same change tendency as the hardness shown in Fig. 1. The strengths of Alloys A and B attain maximum and then decrease slightly at the later stage of aging. However, the strength of Alloy C remains stable during a long aging process. When aged at 120 °C for 12 h, three alloys have the best overall mechanical properties. Table 2 shows the mechanical properties of three alloys aged at 120 °C for 12 h.

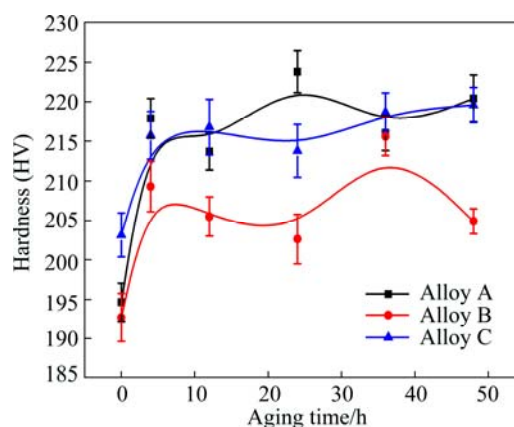


**Fig. 1** Effect of aging time on hardness of Alloys A, B and C

**Table 2** Mechanical properties of Alloy A, B and C aged at 120 °C for 12 h

Alloy	$\sigma_b$ /MPa	$\sigma_{0.2}$ /MPa	$\delta$ /%
A	736	695.5	7
B	711	674	12.5
C	740.5	707.5	13

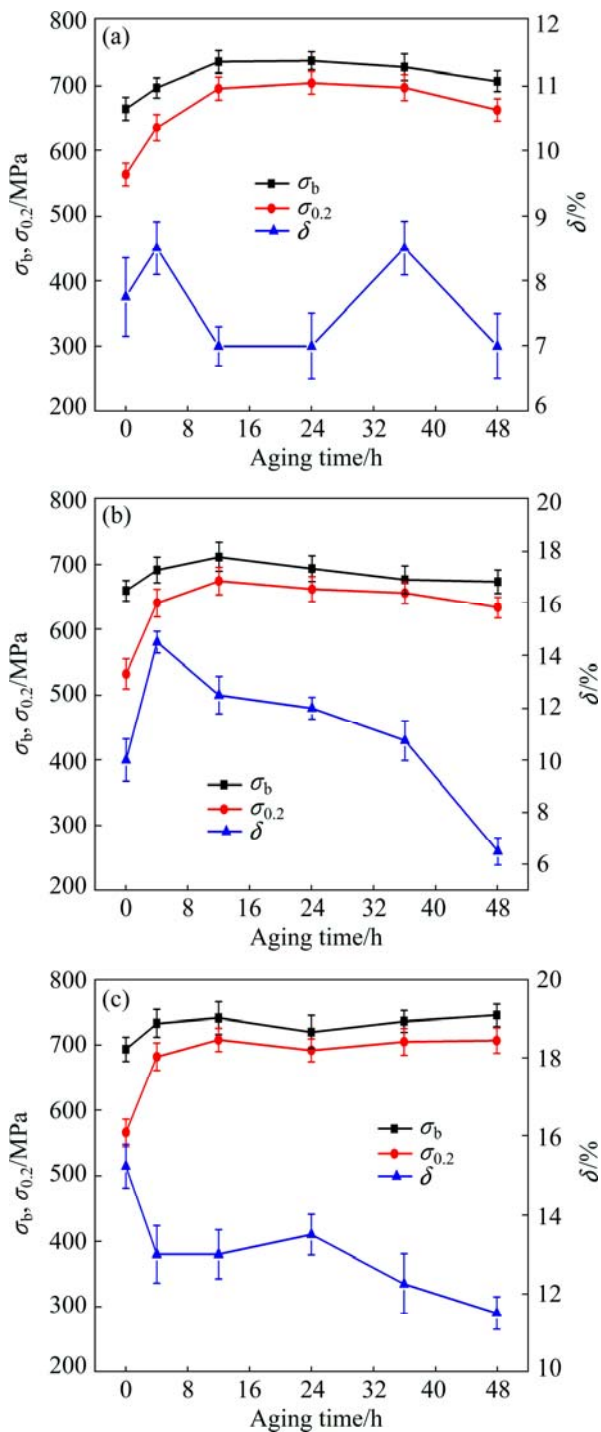


Fig. 2 Mechanical properties of Alloys A (a), B (b) and C (c) at different aging time

### 3.2 Microstructure

Figure 3 shows TEM images of Alloy A aged at 120 °C for 12 h. Figures 3(b) and (c) show the dark field (DF) TEM images along the  $\langle 001 \rangle$  axis of Al matrix and Fig. 3(e) shows the bright field (BF) TEM image along the  $\langle 112 \rangle$  axis of Al matrix. From Figs. 3(b), (c) and (e), it can be seen that the precipitates distribute finely and homogeneously in the matrix; EDS results at Point A in

Fig. 3(c) are listed in Table 3.

The precipitates were identified by the selected area electron diffraction (SAED) along different directions. Figures 3(a) and (d) show the SAED images along directions of  $\langle 001 \rangle$  and  $\langle 112 \rangle$  of Al matrix. Strong diffraction features of  $\eta'$  phases are only observed in Fig. 3(a), such as diffraction spots at  $1/3\{220\}$  and  $2/3\{220\}$  positions in  $\langle 001 \rangle$  and  $\langle 112 \rangle$  directions. Some diffraction spots and weak streak along  $\{111\}$  direction at  $1/3\{220\}$  and  $2/3\{220\}$  positions are observed in  $\langle 112 \rangle$  direction. In Fig. 3(d), it is easy to observe the diffraction feature of GPII zones and the diffraction spots near  $1/2\{311\}$  in  $\langle 112 \rangle$  direction. Hence, the two SAED images show that there are only GPII zone and  $\eta'$  phase in the alloy after aging at 120 °C for 12 h.

Large-scale particles are also observed in Fig. 3(c). According to the results of energy dispersive X-ray spectroscopy (EDS), these particles are rich in Mn, Cu and Al, and the chemical composition of these large-scale particles is similar to  $T(\text{Al}_{20}\text{Cu}_2\text{Mn}_3)$  phase, whether they are  $T$  phase needs to be further investigated.

Figure 4 shows TEM images of Alloy B aged at 120 °C for 12 h. Figures 4(b) and (d) are the BF TEM images along  $\langle 001 \rangle$  axis and  $\langle 112 \rangle$  axis of Al matrix. From the bright field images, a lot of darkly round precipitates are observed. Also, some small round precipitates with a diameter about 25 nm distribute randomly in the matrix, as indicated by arrow in Fig. 4(d). These precipitates can be identified as  $\eta'$  phase according to SAED images.

Figures 4(a) and (c) show the SAED images corresponding to Figs. 4(b) and (d), respectively. There are no obvious GPI and GPII diffraction features in the patterns, only diffraction features of  $\eta'$  phases can be observed, shown as diffraction spots at  $1/3\{220\}$  and  $2/3\{220\}$  positions in  $\langle 001 \rangle$  direction, and some diffraction spots and weak streak along  $\{111\}$  direction at  $1/3\{220\}$  and  $2/3\{220\}$  positions in  $\langle 112 \rangle$  direction. Meanwhile, the diffraction feature of  $\text{Al}_3\text{Zr}$  can be observed in Fig. 4(c), such as diffraction spots along  $\{111\}$  direction at  $1/2\{220\}$  position in the  $\langle 112 \rangle$  direction. Through the SAED images, the fine darkly round precipitates in Figs. 4(b) and (d) can be identified as  $\eta'$  phase and the round precipitates with a diameter of about 25 nm indicated by arrow in Fig. 4(d) can be identified as  $\text{Al}_3\text{Zr}$  particle. Therefore, the main precipitate in Alloy B aged at 120 °C for 12 h is  $\eta'$  phase.

Figure 5 shows TEM images of Alloy C aged at 120 °C for 12 h. Figures 5(b) and (d) show BF TEM images along  $\langle 001 \rangle$  axis and  $\langle 112 \rangle$  axis of Al matrix. Figures 5(a) and (c) show the SAED images corresponding to Figs. 5(b) and (d), respectively. In Fig. 5(a), diffraction spots at  $\{1, (2n+1)/4, 0\}$  along  $\langle 001 \rangle$  axis are observed, which indicates the existence of GPI

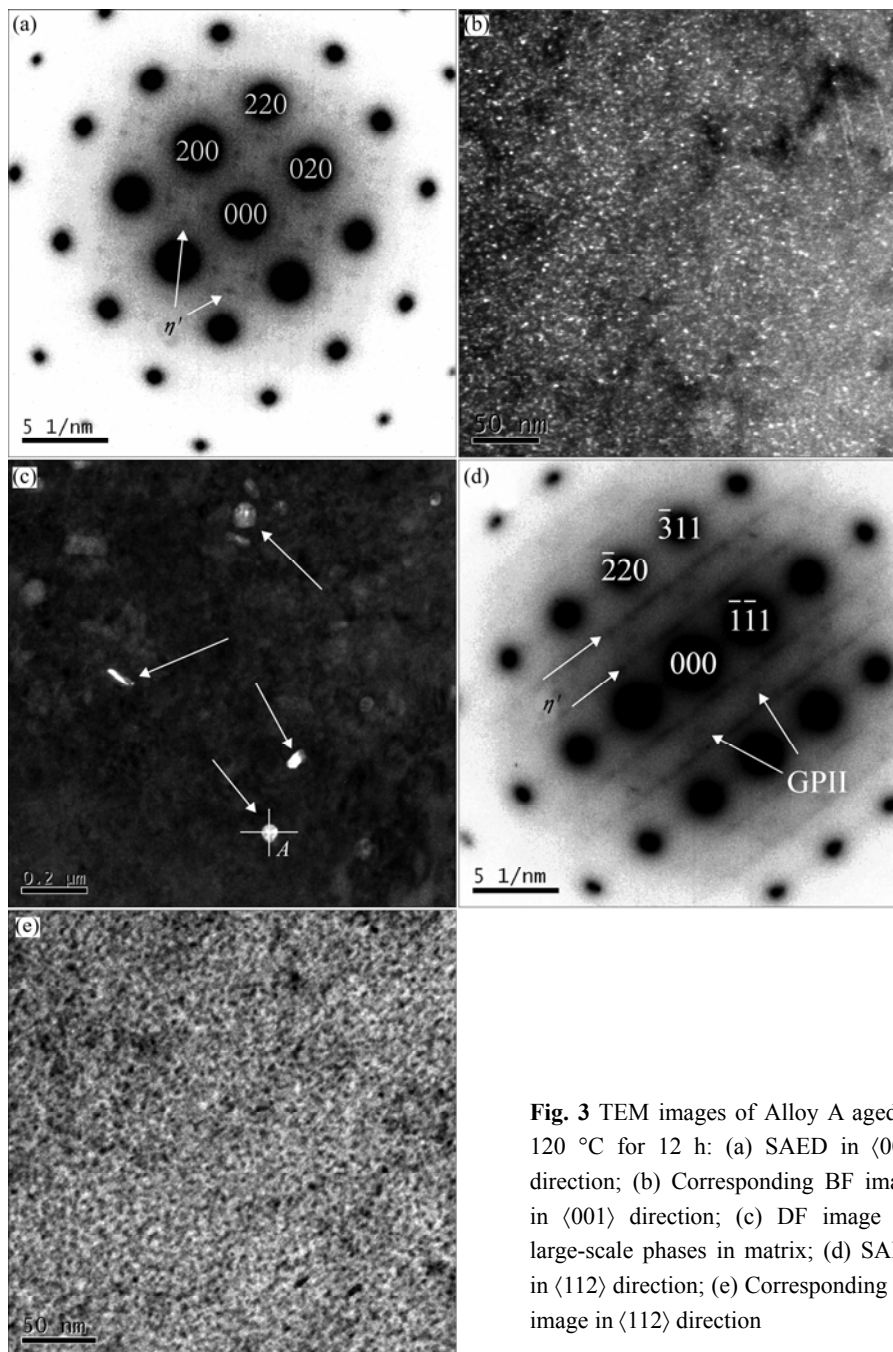


**Fig. 3** TEM images of Alloy A aged at 120 °C for 12 h: (a) SAED in  $\langle 001 \rangle$  direction; (b) Corresponding BF image in  $\langle 001 \rangle$  direction; (c) DF image for large-scale phases in matrix; (d) SAED in  $\langle 112 \rangle$  direction; (e) Corresponding BF image in  $\langle 112 \rangle$  direction

**Table 3** EDS results at Point A in Fig. 3(c)

Element	w/%	x/%
Al	47.66	62.14
Mn	19.71	12.62
Cu	14.21	7.86
Zn	4.48	2.41
Fe	3.95	2.48
Ni	3.11	1.86
Cr	2.42	1.63
F	2.22	4.12
O	2.19	4.83

zones. Strong diffraction spots at  $1/2\{200\}$  and  $1/2\{220\}$  positions are ascribed to  $\text{Al}_3\text{Zr}$  dispersoids and diffraction spots at  $1/3\{220\}$  and  $2/3\{220\}$  positions in  $\langle 001 \rangle$  direction are the diffraction features of  $\eta'$  phases. In Fig. 5(c), it is obvious to observe the diffraction features of GPII zone,  $\eta'$  phases and  $\text{Al}_3\text{Zr}$  dispersoids. Hence, the dark small round precipitates in Figs. 5(b) and (d) can be identified as  $\eta'$  phase, and large dark round particles can be identified as  $\text{Al}_3\text{Zr}$  according to corresponding SAED images. As a result, the main precipitates in Alloy C aged at 120 °C for 12 h are identified as GPI, GPII zone and  $\eta'$  phase.

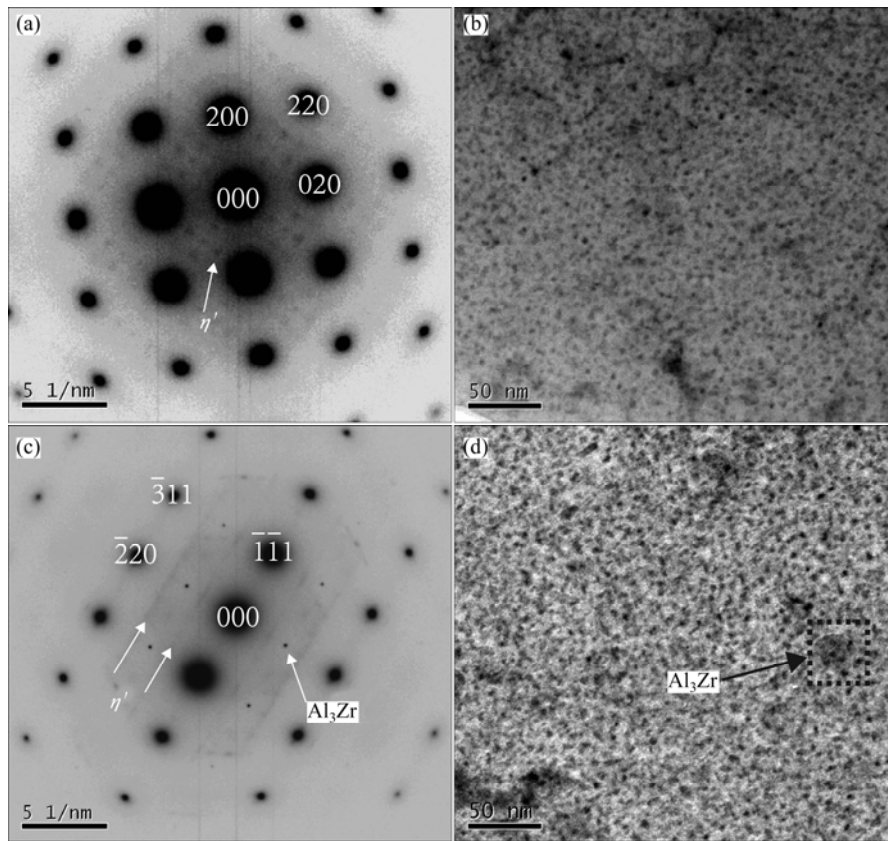


**Fig. 4** TEM images of Alloy B aged at 120 °C for 12 h: (a) SAED in  $\langle 001 \rangle$  direction; (b) Corresponding BF image in  $\langle 001 \rangle$  direction; (c) SAED in  $\langle 112 \rangle$  direction; (d) Corresponding BF image in  $\langle 112 \rangle$  direction

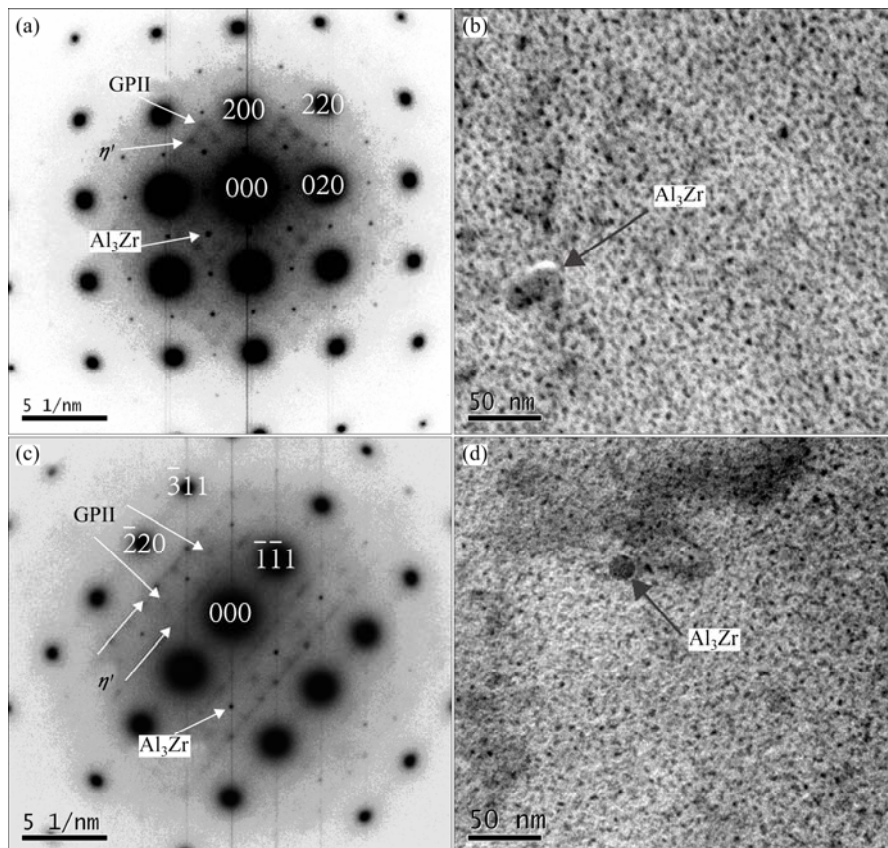


**Fig. 5** TEM images of Alloy C aged at 120 °C for 12 h: (a) SAED in  $\langle 001 \rangle$  direction; (b) Corresponding BF image in  $\langle 001 \rangle$  direction; (c) SAED in  $\langle 112 \rangle$  direction; (d) Corresponding BF image in  $\langle 112 \rangle$  direction

In the last few years, some researchers [16,17] have reported that early-stage Guinier–Preston ( $GP-\eta_p$ ) zones and intermediate phase ( $\eta$ -precursor) could exist in some Al–Zn–Mg–(Cu) alloys. However, in the present study, it was hard to find other early-stage Guinier–Preston ( $GP-\eta_p$ ) zones and intermediate phase ( $\eta$ -precursor).

Figure 6 shows the TEM images of grain boundaries in three alloys. It is obvious to see that coarse precipitates form at grain boundaries in Alloy A, and coarse second phase can also be seen in the interior of grains in Alloy A. While for Alloys B and C, the grain

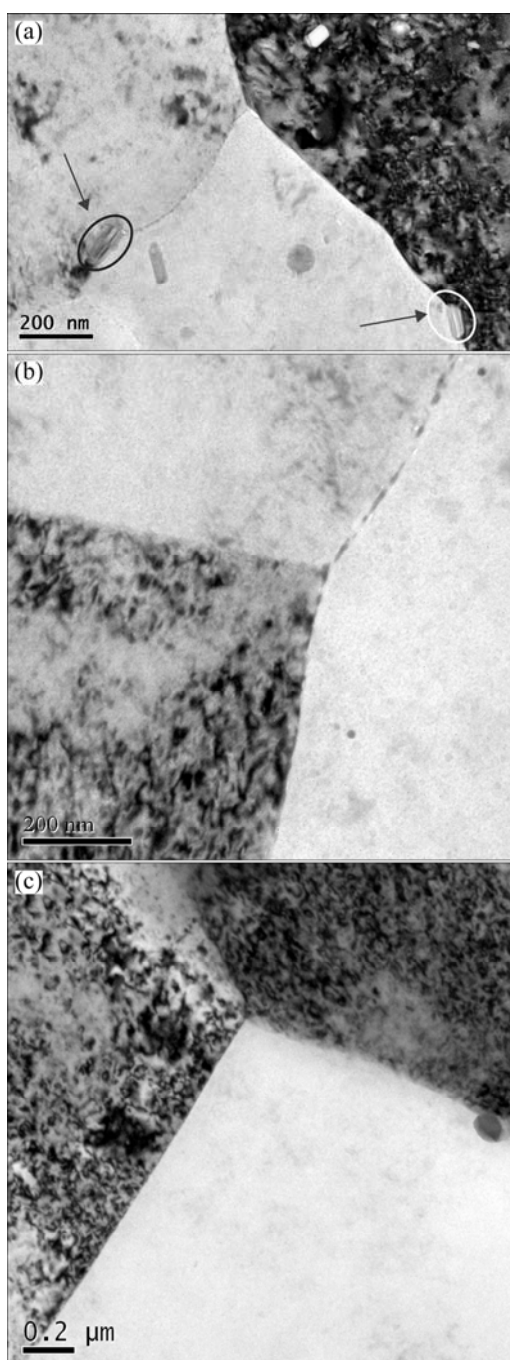


**Fig. 6** TEM images of grain boundaries: (a) Alloy A; (b) Alloy B; (c) Alloy C

boundaries are quite clear and straight, and no large second phase particle can be found within the grain or at grain boundaries.

## 4 Discussion

### 4.1 Influence of aging process on mechanical properties

The hardness and strength of three alloys increase sharply at the early stage of aging process at 120 °C. This phenomenon can be explained by the decomposition of the super-saturated solid solution and the formation of precipitates. As the whole content of alloying element is about 10 %, it is easy for super-saturated solid solution to decompose. Meanwhile, the aging response of Al–Zn–Mg–Cu-based alloys is very significant. As a result, three alloys exhibit very strong strengthening effect after aging. The aging process is related to the formation and coarsening of precipitates. At the early stage of aging process, only coherent metastable GPI and GPII form, and during this stage, the nucleation rate of coherent phases is higher than their growth rate, hence, the hardness of alloys increases sharply. With the increase of aging time, coherent phase transforms to semi-coherent phase like  $\eta'$ , the existence of coherent phase and semi-coherent phase leads to a higher strength of alloys. At the middle stage of aging process, the nucleation rate of precipitates and their growth rate are almost equal, so the strength of alloys keeps stable at high level. At over-aging stage, the hardness and strength of alloys begin to decrease with the increase of aging time. This phenomenon is attributed to the coarsening of semi-coherent phase and the formation of incoherent equilibrium phase.

### 4.2 Influence of precipitates at grain boundary on mechanical properties

The precipitates at grain boundaries have effective influence on mechanical properties of the alloy. As shown in Fig. 6, coarse second phase particles form in grain and at grain boundaries in Alloy A. In Alloys B and C, there are no obvious coarse precipitates at grain boundary or in interior of the grain. As it is well known, the coarse precipitates at grain boundary decrease the mechanical properties of the alloy. For example, it can lead to low grain boundary strength and the tendency of intergranular fracture, and the precipitates at grain boundary result in inhomogeneous plastic deformation. Some particles can easily cause dislocation piling up and stress concentration during deformation. The interface between these particles and grain boundary can be the nucleation site for voids. As a result, Alloy A has the lowest elongation among three alloys. As a contrast, the

grain boundaries of Alloys B and C are clear and fine, and there are no coarse second phase particles at grain boundary. So, the elongations of Alloys B and C are higher than that of Alloy A.

#### 4.3 Influence of alloying elements on mechanical properties

In Fig. 2, it is obvious to see that the tensile strength and yield strength of Alloys A and C keep a high level during the whole aging process. According to the TEM images of Alloys A and C, it is seen that GP zones and  $\eta'$  phase are the main precipitates in Alloys A and C after aging at 120 °C for 12 h, meanwhile, the precipitates in the alloy are finely dispersed and distributed homogeneously. So the fine and homogeneous distribution of the precipitates leads to high strength of Alloys A and C. The Zn content in Alloy C is higher than that in Alloy A, and high Zn content increases the volume fraction of precipitates during aging. As shown as Figs. 2(a) and (c), after aging at 120 °C for 24 h, the strength of Alloy A begins to decrease with the increase of aging time; however, the strength of Alloy C still keeps stable level. This indicates that the increase of Zn content improves the strength of alloy and promotes the strength keeping stable during a long aging process.

In Alloy B, the main strengthening phase is metastable  $\eta'$ , but GPII zone and GPI zone are not observed. The strengthening effect of a single precipitate is weaker than the combinative strengthening effect of several precipitates, so, Alloy B has the lowest tensile strength among the three alloys. Further reason may be that Alloy B has high Cu content, and FAN et al [18] showed that coarse  $S$  ( $Al_2CuMg$ ) phase exists in Al–Zn–Mg–Cu-based alloys which have a high content of Cu, and the formation of coarse  $S$  phases may decrease the supersaturated degree of the matrix by consuming a lot of Cu and Mg atoms after quenching. Therefore, no enough precipitates form during aging and lead to relatively low strength of Alloy B among the three alloys.

The Mn content of Alloy A is about 0.3% (mass fraction), and the coarse precipitates which are rich in Al, Cu and Mn are observed in Alloy A, as shown in Fig. 3(c). On the one hand, the phase which contains Mn can effectively inhibit recrystallization and improve the mechanical properties of the alloy [19,20]. On the other hand, it is easy to promote the formation of tiny voids at the interface between the phase and the matrix. The tiny voids are the reason for crack initiation and can accelerate the growth of crack when the alloy is in service [21]. So, Alloy A has higher tensile strength and lower elongation.

## 5 Conclusions

1) Alloys A, B and C exhibit strong aging strengthening effect. The optimal heat treatment for the three alloys is as follows: solution treatment at 450 °C for 2 h followed by 470 °C for 1 h, then water quenching and aging at 120 °C for 12 h. The tensile strength, yield strength and elongation for Alloys A, B and C are 736 MPa, 695.5 MPa and 7%; 711 MPa, 674 MPa and 12.5%; and 740.5 MPa, 707.5 MPa and 13%, respectively.

2) The dominant strengthening phases in Alloy A are GPII zone and  $\eta'$  phase, the main precipitates in Alloy B is  $\eta'$  phase, and the main precipitations in Alloy C are GPI zone, GPII zone and  $\eta'$  phase.

3) The increase of Zn content leads to the improvement of the strength of the alloy. The increase of Cu content improves the elongation but slightly decreases the strength. Large particles formed by the increase of Mn content induce the decrease of elongation.

## References

- [1] STAIR M A, MCINTURFF T L. Casing and tubing design considerations for deep sour-gas wells [J]. SPE Drilling Engineering, 1986, 1(3): 221–232.
- [2] YAN Tai-ning, XUE Wei, LAN Kai. High reliability aluminum alloy drill pipe and its application in super-deep wells and extended-reach wells [J]. Geological Science and Technology Information, 2010, 29(1): 112–115. (in Chinese)
- [3] ROMETSCH P A, ZHANG Y, KNIGHT S. Heat treatment of 7xxx series aluminium alloys — Some recent developments [J]. Transactions of Nonferrous Metals Society of China, 2014, 24(7): 2003–2017.
- [4] LIAO Yu-guo, HAN Xiao-qi, ZENG Miao-xia, JIN Man. Influence of Cu on microstructure and tensile properties of 7xxx series aluminum alloy [J]. Materials & Design B, 2015, 66: 581–586.
- [5] HE Yong-dong, ZHANG Xin-ming, YOU Jiang-hai. Effect of minor Sc and Zr on microstructure and mechanical properties of Al–Zn–Mg–Cu alloy [J]. Transaction of Nonferrous Metals Society of China, 2006, 16(5): 1228–1235.
- [6] ZOU Liang, PAN Qing-lin, HE Yun-bin, WANG Chang-zhen, LIANG Wen-jie. Effect of minor Sc and Zr addition on microstructures and mechanical properties of Al–Zn–Mg–Cu alloys [J]. Transaction of Nonferrous Metals Society of China, 2007, 17(2): 340–345.
- [7] YANG X B, CHEN J H, LIU J Z, QIN F, XIE J, WU C L. A high-strength AlZnMg alloy hardened by the  $T$ -phase precipitates [J]. Journal of Alloys and Compounds, 2014, 610: 69–73.
- [8] FAN Xi-gang, JIANG Da-ming, MENG Qing-chang, LAI Zhong-hong, ZHANG Xin-mei. Characterization of precipitation microstructure and properties of 7150 aluminium alloy [J]. Materials Science and Engineering A, 2006, 427(1–2): 130–135.
- [9] STILLER K, WARREN P J, HANSEN V, ANGENETE J, GJØNNES J. Investigation of precipitation in an Al–Zn–Mg alloy after two-step ageing treatment at 100 °C and 150 °C [J]. Materials Science and Engineering A, 1999, 270(1): 55–63.

- [10] WU Xian-zhe, XIAO Dai-hong, ZHU Zhe-min, LI Xiu-xiu, CHEN Kang-hua. Effects of Cu/Mg ratio on microstructure and properties of AA7085 alloys [J]. Transactions of Nonferrous Metals Society of China, 2014, 24(7): 2054–2060.
- [11] LENDVAI J, HONYEK G, KOVACS I. Dissolution of second phases in an Al–Zn–Mg alloy investigated by calorimetric method [J]. Scripta Metallurgica, 1979, 13(7): 593–594.
- [12] GANG S, CERESO A. Early-stage precipitation in Al–Zn–Mg–Cu alloy (7050) [J]. Acta Materialia, 2004, 52(15): 4503–4516.
- [13] ZANG Jin-xin, ZHANG Kun, DAI Sheng-long. Precipitation behavior and properties of a new high strength Al–Zn–Mg–Cu alloy [J]. Transaction of Nonferrous Metals Society of China, 2012, 22(11): 2638–2644.
- [14] LI Xi-wu, XIONG Bai-qing, ZHANG Yong-an, HUA Cheng, LI Zhi-hui, ZHU Bao-hong, LIU Hong-wei. One-step ageing behavior of a novel Al–7.5Zn–1.7Mg–1.4Cu–0.12Zr alloy [J]. Rare Metal Materials and Engineering, 2009, 38(9): 1589–1593. (in Chinese)
- [15] WANG Tao, YIN Zhi-min, SHEN Kai, LI Jie, HUANG Ji-wu. Single-aging characteristics of 7055 aluminum alloy [J]. Transaction of Nonferrous Metals Society of China, 2007, 17(3): 548–552.
- [16] LIU J Z, CHEN J H, YANG X B, REN S, WU C L, XU H Y, ZOU J. Revisiting the precipitation sequence in Al–Zn–Mg-based alloys by high-resolution transmission electron microscopy [J]. Scripta Materialia, 2010, 63(11): 1061–1064.
- [17] LIU J Z, CHEN J H, LIU Z R, WU C L. Fine precipitation scenarios of AlZnMg(Cu) alloys revealed by advanced atomic-resolution electron microscopy study: Part II: Fine precipitation scenarios in AlZnMg(Cu) alloys [J]. Materials Characterization, 2015, 99: 142–149.
- [18] FAN Xi-gang, JIANG Da-ming, SHAN Chang-zhi, LI Nian-kui, SUN Zhao-xia. Effect of copper content on the properties and fracture behavior in Al–Zn–Mg–Cu alloys [J]. Light Alloy Fabrication Technology, 2006, 34(2): 31–35. (in Chinese)
- [19] PRINCE K C, MARTIN J W. The effects of dispersoids upon the micromechanisms of crack propagation in Al–Mg–Si alloys [J]. Acta Metallurgica, 1979, 27(8): 1401–1408.
- [20] WALSH J A, JATA K V, STARKE E A Jr. The influence of Mn dispersoid content and stress state on ductile fracture of 2134 type Al alloys [J]. Acta Metallurgica, 1989, 37(11): 2861–2871.
- [21] BECKER R, SMELSER R E. Simulation of strain localization and fracture between holes in an aluminum sheet [J]. Journal of the Mechanics and Physics of Solids, 1994, 42(5): 773–796.

## 石油钻杆用高强 Al–Zn–Mg–Cu 系 铝合金的显微组织和力学性能

冯春<sup>1,2</sup>, 寿文彬<sup>3</sup>, 刘会群<sup>3</sup>, 易丹青<sup>3</sup>, 冯耀荣<sup>1,2</sup>

1. 中国石油天然气集团公司 管材研究所, 西安 710065;
2. 中国石油天然气集团公司 石油管工程重点实验室, 西安 710065;
3. 中南大学 材料科学与工程学院, 长沙 410083

**摘要:** 采用维氏硬度测试、拉伸性能测试、透射电子显微镜(TEM)研究 3 种石油钻杆用 Al–Zn–Mg–Cu 系合金 (合金 A: Al–6.9Zn–2.3Mg–1.7Cu–0.3Mn–0.17Cr, 合金 B: Al–8.0Zn–2.3Mg–2.6Cu–0.2Zr, 合金 C: Al–8.0Zn–2.3Mg–1.8Cu–0.18Zr) 的显微组织和力学性能。结果表明, 经(450 °C, 2 h)+(470 °C, 1 h)固溶处理及 120 °C 时效 12 h 后, A、B 和 C 3 种合金的抗拉强度、屈服强度和伸长率分别达到 736 MPa、695.5 MPa 和 7%; 711 MPa, 674 MPa 和 12.5%; 740.5 MPa, 707.5 MPa 和 13%。合金 A 的强化相为细小弥散分布的 GPII 区和  $\eta'$  相; 合金 B 的强化相为  $\eta'$  相; 合金 C 的强化相为 GPI 区、GPII 区和  $\eta'$  相, 这是合金 C 具有较佳综合性能的原因。增加 Zn 含量有利于提高合金强度; 增加 Cu 含量使合金强度略有下降, 伸长率上升; 增加 Mn 含量使合金基体内形成尺寸较大的第二相粒子, 从而导致合金塑性的降低。

**关键词:** Al–Zn–Mg–Cu 系合金; 时效时间; 强化相; 显微组织; 力学性能

(Edited by Wei-ping CHEN)